PCCP

Accepted Manuscript

ROYAL SOCIETY OF CHEMISTRY

www.rsc.org/pccp

Physical Chemistry Chemical Physics
CREATED USING THE RSC LaTeX PCCP ARTICLE TEMPLATE – SEE www.rsc.org/electronicfiles FOR DETAILS
ARTICLE TYPE www. rsc.org/xxxxxx | XXXXXXXX

The effects of thermal and electric fields on the electronic structures of silicene

Chao Lian and Jun Ni*

Received Xth XXXXXXXXXX 20XX, Accepted Xth XXXXXXXXX 20XX
First published on the web Xth XXXXXXXXXX 200X
DOI: 10.1039/b000000x

We have investigated the effects of thermal and electric fields on the electronic properties of silicene. **The effects are studied by a statistical analysis of canonical ensembles combined with the tight binding method. The tight binding parameters of silicene are obtained by fitting with the first principles results.** We analysis the statistics of the gaps, the masses of the Dirac fermions and the effective speeds of light as a function of the cell dimension N. We show that the symmetry breaking caused by the buckling disorder in the thermal field alter the band structures of the silicene with small cells greatly. However, the buckling variation of any atom is compensated by other atoms in a large cell. Thus the band structure features near the Fermi energy in the pristine silicene are still protected by the sublattice symmetry in thermal field. Moreover, the thermal field enhances the effect of electric field to generate a band gap. The randomly buckled silicene needs much smaller electric field than the pristine silicene. The higher temperature corresponds to a larger gap under the same electric field. All these features make silicene a better candidate for electronic devices at ambient temperature.

1 Introduction

A novel two-dimensional material, silicene, is experimentally synthesised and observed on silver and zirconium diboride substrate.[1–17] Many researches have been carried on the electronic properties of silicene, including the free standing silicene[18–26], the silicene on substrate[27–31] and the silicene bilayer[32–37]. Silicene own most advantages that graphene has such as the high mobility of Dirac fermions. Furthermore, the microelectronic techniques is highly developed on silicon materials, which makes the silicene more compatible to build electronic devices such as field effect transistor(FET).

Most recently, the silicene FET is built at room temperature.[38] A great effort is needed to improve the relatively low on/off ratio of silicene FET. However, most computational researches of silicene are concentrated on the zero-temperature phenomena. There are many differences when a thermal field is applied on two dimensional materials. The structural modification is conspicuous. One example is the intrinsic ripples in graphene.[39] For silicene, because the energy cost of the changes in buckling height is small, a low energy thermal field is sufficient to break the ordered buckling state.[2,40,41] Thus the change of the buckling heights in a thermal field is the most obvious and also an unique factor which is different from that of other materials such as graphene and boron nitride. At room temperature ($\sim 300K$), the buckling configurations are more likely to be disordered rather than form a regular pattern as it is at 0K. The disordered buckling will lead to a difference in the electronic properties.[23,42] This difference may lead to unpredicted behavior of the silicene FET devices. Therefore, how will the thermal field affect the band structure of silicene is an important issue but not yet discussed.

In this work, we investigate the effect of thermal field on the electronic properties of silicene. We find that the vibration in buckling height is the main Goldstone mode while the in-plane movement is frozen at room temperature. This effect is studied using a canonical ensemble of silicene structures, which are randomly buckled. The analysis of the variation of the gaps, the masses of the Dirac fermions and the effective speeds of light, show the effect of buckling disorder is smeared out as the periodicity goes infinite. Therefore, the randomly buckled silicene will share nearly the same electric properties as pristine silicene. Moreover, the randomly buckled silicene need much smaller electric field to generate the same gap and the higher temperature corresponds to a larger gap under the same electric field. All these features make silicene a better candidate for electronic devices at room temperature.

This article is organized as follows: Section 2 describes the details of the first principles method, the tight-binding method and the ensemble model. Section 3 is the results and discussions: Section 3.1 describes the general features of the energy bands of random buckled silicene. Section 3.2 describes the statistics of the gap, mass and the effective speed of light, respectively; Section 3.3 studies the effect of the electric field on

Address, Department of Physics and State Key Laboratory of Low-Dimensional Quantum Physics, Tsinghua University, Beijing 100084, P.R.China. Fax: (8610)62781604; Tel: +8601062772781; E-mail: junni@mail.tsinghua.edu.cn

randomly buckled silicene at different temperatures. Section 4 is the summary.

2 Methods and Models

The first principles calculations are performed with the Vienna Ab initio Simulation Package (VASP).[43–45] The projector augmented-waves method[46] and Perdew-Burke-Ernzerhof exchange-correlation[47] are used. The plane-wave cutoff energy is set to be 250 eV. The vacuum space is set to be larger than 15 Å. The Brillouin zone is sampled using Monkhorst-Pack scheme[48]. We use a k-point mesh of $18\times18\times1$ for the 1×1 unit cell, $6\times6\times1$ for the 3×3 and 4×4 supercell in the self-consistent calculations. Using the conjugate gradient method, the positions of atoms are optimized until the convergence of the force on each atoms is less than 0.005 eV/Å.

To simulate a statistical ensemble, a large sample of structures are calculated. The calculations are nearly impossible to be accomplished using the density-functional method. Instead, we use the Slater-Koster tight-binding method[49] which has been generally recognized as an efficient and a sufficiently accurate method to study the group-IV nanostructures.[50–56]

The Slater-Koster Hamiltonian has the form

$$H=\begin{pmatrix} H_{1,1} & H_{1,2} & \cdots & H_{1,M-1} & H_{1,M} \\ H_{2,1} & H_{2,2} & \cdots & H_{1,M-1} & H_{1,M} \\ \vdots & \vdots & \ddots & \vdots & \vdots \\ H_{M-1,1} & H_{M-1,2} & \cdots & H_{M-1,M-1} & H_{M-1,M} \\ H_{M,1} & H_{M,2} & \cdots & H_{M,M-1} & H_{M,M} \end{pmatrix}, \tag{1}$$

where $H_{i,j}=H_{j,i}^{\dagger}$ is a matrix describing the interaction between atom i and atom j, and M denotes the total number of atoms in the cell. We consider four atomic orbitals of silicon atom: s, p_x, p_y and p_z, thus $H_{i,j}$ is a 4×4 matrix. Explicitly,

$$H_{i,i}=\begin{pmatrix} \varepsilon_s & 0 & 0 & 0 \\ 0 & \varepsilon_p & 0 & 0 \\ 0 & 0 & \varepsilon_p & 0 \\ 0 & 0 & 0 & \varepsilon_p \end{pmatrix} \tag{2}$$

is the expression of the diagonal submatrix, and

$$H_{i,j}=\begin{pmatrix} h_{s^i s^j} & h_{s^i p_x^j} & h_{s^i p_y^j} & h_{s^i p_z^j} \\ h_{p_x^i s^j} & h_{p_x^i p_x^j} & h_{p_x^i p_y^j} & h_{p_x^i p_z^j} \\ h_{p_y^i s^j} & h_{p_y^i p_x^j} & h_{p_y^i p_y^j} & h_{p_y^i p_z^j} \\ h_{p_z^i s^j} & h_{p_z^i p_x^j} & h_{p_z^i p_y^j} & h_{p_z^i p_z^j} \end{pmatrix} (i\neq j) \tag{3}$$

is the expression of the off-diagonal submatrix, where

$$h_{\alpha^i,\beta^j}=\sum_{i=1}^{N}\sum_{j\neq i}^{N}\mu_{\alpha^i,\beta^j}(|\mathbf{r}_j-\mathbf{r}_i|)\exp[i\mathbf{k}\cdot(\mathbf{r}_j-\mathbf{r}_i)] \tag{4}$$

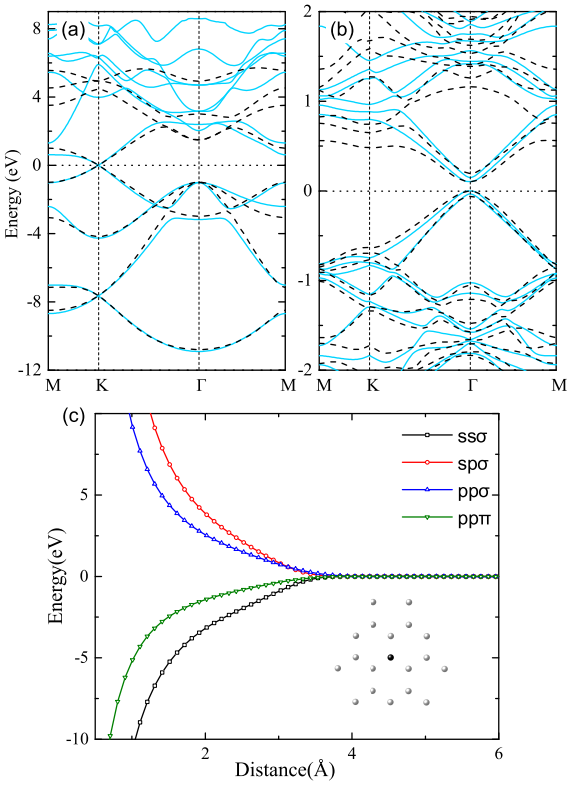

Fig. 1 (Color online) The energy bands of (a) 1×1 pristine silicene and (b) 3×3 randomly buckled silicene. The solid line is the density-functional result and the dash line is the tight-binding result. The Fermi energy is set to zero. (c) The hooping parameters of $ss\sigma$ (square), $sp\sigma$ (circle), $pp\sigma$ (up-triangle), $pp\pi$ (down-triangle) as a function of distance. Inset: The schematic of the neighboring atoms within cut-off radius. The black ball represents the selected atom, and the grey balls represent the interacting neighboring atoms.

is the hopping integral between the orbital α of the atom i and the orbital β of the atom j. The expression of μ_{α^i,β^j} is shown in Table. 1.

Since the heights of buckling are different, the hooping parameters $V_{ss\sigma}$, $V_{sp\sigma}$, $V_{pp\sigma}$, $V_{pp\pi}$ are not constants but a function of r. We use the Goodwin[57] form to describe the hooping parameters as a function of distance:

$$V_{\mu\nu\lambda}(r)=V_0\left(\frac{r_0}{r_c}\right)^n\exp\left\{n\left[\left(\frac{r_0}{r_c}\right)^{n_c}-\left(\frac{r}{r_c}\right)^{n_c}\right]\right\} \tag{5}$$

where V_0, r_0, r_c, n, n_c are parameters listed in Table 2. These parameters together with ε_s and ε_p in Eq. (2) are fitted with first-principles energy band of 1×1 silicene cell, as shown in Fig. 1(a). **Since the parameters are used to reproduce not only the band structure of the prinstine silicene but also that of the randomly buckled structures, we need to adapt the parameters to describe both the prinstine silicene**

Table 1 The Slater-Koster expression[49] of the μ_{m^α,n^β} of in Eq. (4). The V_{ss}, $V_{sp\sigma}$, $V_{pp\sigma}$ and $V_{pp\pi}$ are the tight-binding parameters. Here $l=(\mathbf{r}_j-\mathbf{r}_i)\cdot\hat{\mathbf{x}}$, $m=(\mathbf{r}_j-\mathbf{r}_i)\cdot\hat{\mathbf{y}}$ and $n=(\mathbf{r}_j-\mathbf{r}_i)\cdot\hat{\mathbf{z}}$

	s^j	p_x^j	p_y^j	p_z^j
s^i	$V_{ss\sigma}$	$lV_{sp\sigma}$	$mV_{sp\sigma}$	$nV_{sp\sigma}$
p_x^i	$-lV_{sp\sigma}$	$l^2V_{sp\sigma}+(1-l^2)V_{sp\pi}$	$lm(V_{pp\sigma}-V_{pp\pi})$	$ln(V_{pp\sigma}-V_{pp\pi})$
p_y^i	$-mV_{sp\sigma}$	$lm(V_{pp\sigma}-V_{pp\pi})$	$m^2V_{sp\sigma}+(1-m^2)V_{sp\pi}$	$mn(V_{pp\sigma}-V_{pp\pi})$
p_z^i	$-nV_{sp\sigma}$	$ln(V_{pp\sigma}-V_{pp\pi})$	$mn(V_{pp\sigma}-V_{pp\pi})$	$n^2V_{sp\sigma}+(1-n^2)V_{sp\pi}$

Table 2 The hooping parameters for silicene in the Goodwin form.[57] The unit is eV. The orbital energies $\varepsilon_s=-3.21eV$, $\varepsilon_p=0.0eV$.

	V_0	r_0	r_c	n	n_c
$ss\sigma$	-2.54	2.27	3.37	1.72	9.05
$sp\sigma$	2.95	2.27	3.38	1.97	7.92
$pp\sigma$	2.08	2.27	3.56	1.83	7.18
$pp\pi$	-1.06	2.27	3.43	1.81	7.09

and the randomly buckled silicene accurately. Thus several 1×1 cells with different buckling heights are chosen to minimize the difference between the tight-binding and first-principles results, to ensure the parameters is transferable to study the silicene with different buckling heights. A Nelder-Mead simplex method is used for this parameter optimization.[58]

$V_{\mu\nu\lambda}(r)$ is shown in Fig. 1(c). $V_{\mu\nu\lambda}(r)$ decays rapidly with the increase of inter-atom distance and vanish at $4\mathring{A}$, which means that a pair of atoms with a distance larger than $4\mathring{A}$ has no direct interaction approximately. Thus we set a cut-off radius of $4\mathring{A}$, i.e. the tight-binding calculations include the interaction between a selected atom and its neighbor atoms within $4\mathring{A}$, as shown in Fig. 1.

These parameters are elaborately tested to confirm their accuracy and transferability. Using the parameters fitted from the 1×1 unit cell, we calculate the energy bands of several 3×3 silicene supercells with different buckling configurations, and compare them with the first principles results. One example of these band structures is shown in Fig. 1(b). It shows that this set of parameters is generally accurate to regenerate the band structure near the Fermi energy of randomly buckled structures.

The changes in buckling heights cost a relative small energy compared with those of in-plane displacements(Fig.2(b)). At room temperature, the energy of the thermal field is about $E_{tf}=k_bT=8.62\times105eV/K\times300K\sim25.86meV$. For the 1×1 silicene cell, the buckling heights can change from $-0.67\mathring{A}$ to $0.67\mathring{A}$, while the in-plane displacements can only vary from $-0.07\mathring{A}$ to $0.07\mathring{A}$. For the change of the buckling height of one single silicon atom in the 4×4 silicene cell, the

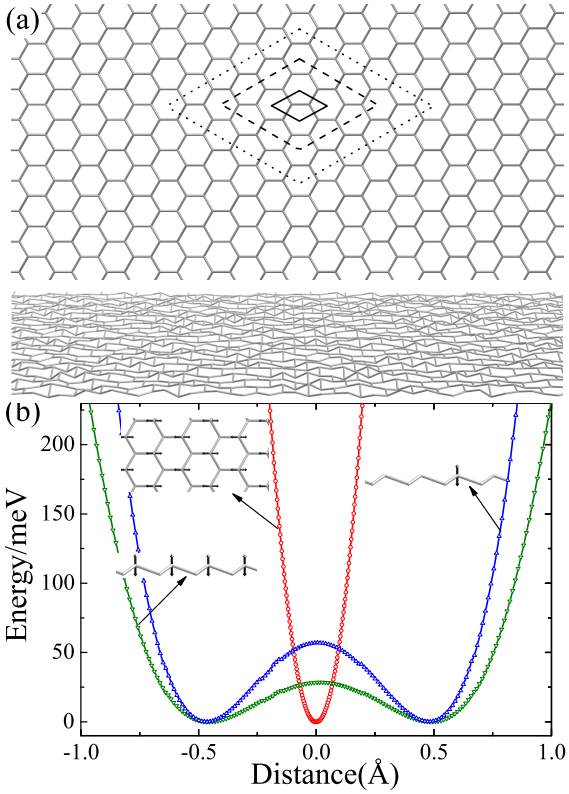

Fig. 2 (Color online) (a) The structure of buckling disorder silicene. The solid/dash/dotted line represent the $1\times1/3\times3/5\times5$ silicene cell. (b) The energies as a function of distance from the first principles calculations. The circle denotes energy as a function of the in-plane displacement from the equilibrium positions. The square denotes the energy as a function of the buckling height of a single silicon atom in the 4×4 silicene cell. The triangle denotes the energy as a function of the buckling height of all the atoms in a specific sublattice.

buckling height can change from $-0.62\AA$ to $0.62\AA$, as shown in Fig.2(b). It means that the buckling changes cost small energy, consistent with the former researches[2,40,41]. For simplicity, we consider only the fluctuations of buckling height and treat the in-plane movement as a frozen dimension.

In our calculations, the periodical boundary condition is applied. The buckling is disordered within the cell but has a periodicity of the supercell. In the finite-size scaling approach, with the height of the basis vector increases, the buckling becomes totally disordered, which depicts the realistic situation. The property of the infinite silicene sheet is obtained using extrapolation as the supercell expands from 1×1 to 12×12. The $N\times N$ silicene cell is shown in Fig. 2(a).

The electronic property of silicene is dependent on the long time average of the electronic structures. At room temperature, there are the flip-flop motions between different buckling phases. Since the realistic silicene material in the thermal field is randomly buckled, the long time average can be described as an ensemble which consists of numerous randomly buckled structures. Thus we simulate a canonical (NVT) ensemble, which consists of numerous structures. We consider 2×10^3 structures for each $N\times N$ cell. **We compare the statistic results with different numbers of configurations to ensure that 2×10^3 configurations are sufficient to simulate a canonical ensemble. As shown in Figure 3(a), the distributions of the band gaps of σ=500 and σ=2000 8×8 silicene structures show little difference. The quantitative comparison is shown in Figure 3(b). We define**

$$\eta=(\Delta_\sigma-\Delta_{\sigma_0})/\Delta_{\sigma_0}, \tag{6}$$

where the Δ_σ is the mean value of the band gaps of σ configurations and Δ_{σ_0} is the mean value of the band gaps of $\sigma_0=2\times10^3$ configurations. It is clear that when σ is larger than 900, the mean values Δ_σ differ within 1% from the mean value of Δ_{σ_0}. Thus, we demonstrate that with $\sigma=2\times10^3$ structures, the statistic error of Δ_{σ_0} is less than 1%. Thus, the 2×10^3 buckled structures are sufficient to reproduce a canonical ensemble. Since the simulated ensemble contains all the statistical properties of the silicene in the thermal field, it includes all the entropy effect.

According to the ensemble theory, the possibility of the structure with energy E is $P\propto\exp(-\beta E)$, where $\beta=(k_BT)^{-1}$ and k_B is the Boltzmann constant. The Metropolis algorithm[59] is used to sample the structures. The structure is accepted with the possibility P.

The cohesive energy E of the structure is evaluated using a simple model.

$$E=\sum_{\langle i,j\rangle}\sum_{m=1}^{9}C_m(Z_i-Z_j)^m, \tag{7}$$

where $\langle i,j\rangle$ is a pair of nearest neighbors in the cell, Z_i-Z_j is the difference in buckling height, and the parameters are

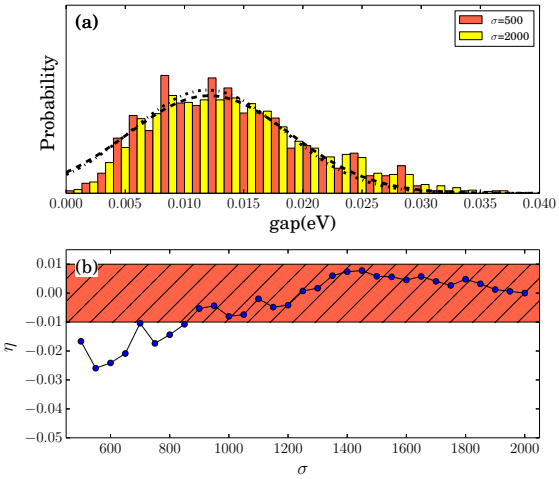

Fig. 3 (Color online) (a) Probability distribution of the band gaps in 8×8 silicene. The dark bars and the light bars denote the statistics of σ=500 and σ=2000 different structures, respectively. The dotted line and dash line denote the fitted Gaussian distributions of σ=500 and σ=2000, respectively. (b) The mean values of the gaps as a function of the number of structures.

obtained as $C_1=3.25, C_2=-170.63, C_3=-122.20, C_4=-331.38, C_5=-1406.53, C_6=773.39, C_7=6111.70, C_8=7269.61, C_9=2813.81$ by fitting with the energy curve in Fig.2(b).

3 Results and Discussions

3.1 General features of energy bands of random buckled silicene

The semimetal feature of silicene is protected by the symmetric AB sublattices. The energy dispersion $E(k)$ of the quasiparticle near Fermi level is Dirac-type[60,61]:

$$E(k)=\pm c\hbar(\vec{k}-\vec{k_0}), \tag{8}$$

where c is the effective velocity of light, $\hbar$ is the Planck constant and $\vec{k_0}$ is the location of the Dirac point in the k space.

When the thermal field randomizes the buckling heights, the original rotatory inversion symmetry of pristine silicene is broken and a band gap is generated. In other words, the disorder produces an intervalley scattering vector, which causes a small band gap in each structure and disturbs the linear dispersion near the Fermi level. It can be viewed as a mass generation in massless Dirac fermions. The dispersion of massive Dirac fermion is described as:

$$E(k)=\pm\sqrt{c^2\hbar^2(\vec{k}-\vec{k_0})^2+(mc^2)^2}, \tag{9}$$

where m is the mass of the Dirac fermion.

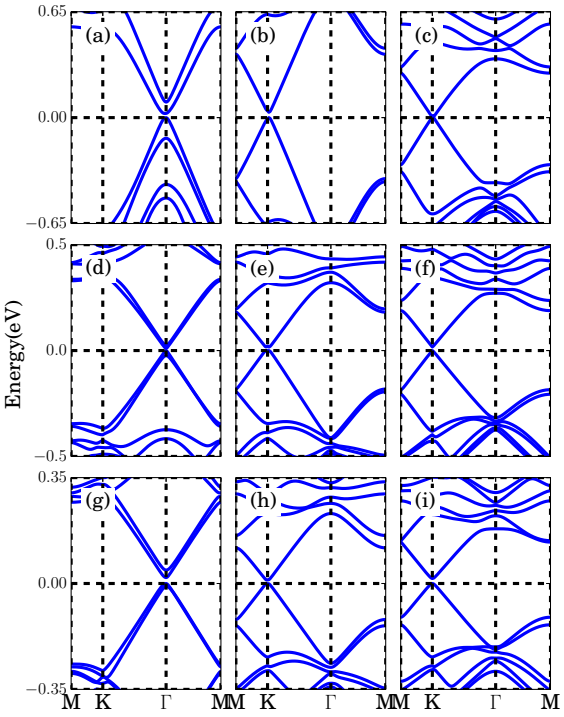

Fig. 4 (Color online) (a-i)Tight-binding energy bands of $N \times N$ silicene near the Fermi level (N=3,4,...,11). The Fermi energy is set to zero.

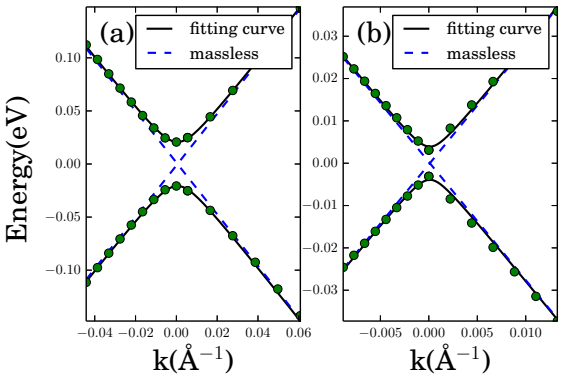

Fig. 5 (Color online) Tight-binding energy bands (circles) and fitting curves (solid lines) of (a) 3×3 and (b) 6×6 silicene near the Fermi level. Dash lines denotes the $E(k)$ curve of massless Dirac fermions.

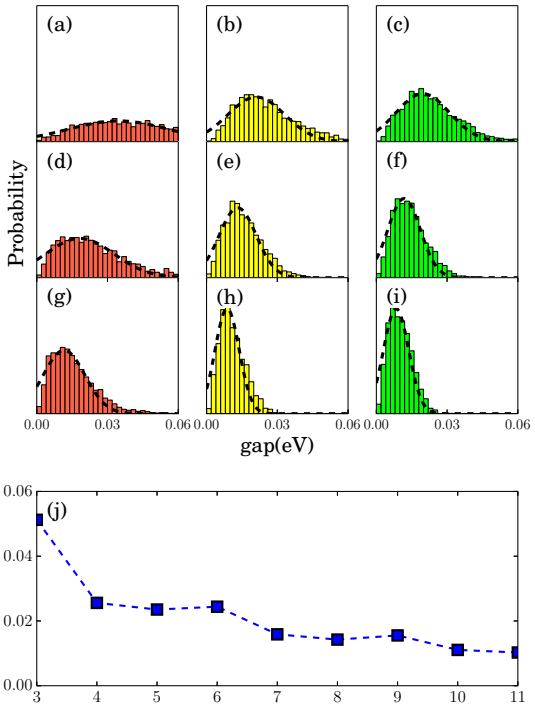

Fig. 6 (Color online) (a-i) Probability distributions of the gaps of $N \times N$ cells (N=3,4,...,11). (j) The mean values of each ensemble.

Figure 4 shows the example of the energy bands of $N \times N$(N=3,4,..,11) supercells. According to the location of the Dirac point in the k space, the $N \times N$ supercells can be divided into two categories. One is $N = 3p$ and the other is $N \neq 3p$, where $p = 1, 2, 3$. For the $N \neq 3p$ supercells, the Dirac point is located at K and K', while for the $3p \times 3p$ supercells, the valleys K and K' are folded into the Γ point. This folding results in significant intervalley scattering and a relative large band gap.

The $E(k)$ of massive Dirac fermions (9) is fitted with the tight-binding band data. As shown in Fig. 5, the tight-binding bands of 3×3 and 6×6 supercell can be well fitted with the function in Eq. (9). The parameters c and m can be obtained for each structure of $N \times N$ supercell.

3.2 Statistics of energy gap, mass and effective speed of light

The band gap $\Delta = 2mc^2$ can be obtained from Eq.(9). We carry a statistic study of the band gaps of each $N \times N$ supercell, as shown in Fig. 6(a-i). When N is small, the peak of the distribution is wide, which means the gaps vary in a large range. For $N = 3$, The intervalley scattering is strong enough to generate a considerable gap (over 100meV). In general, with N increases, the intervalley scattering is weakened.

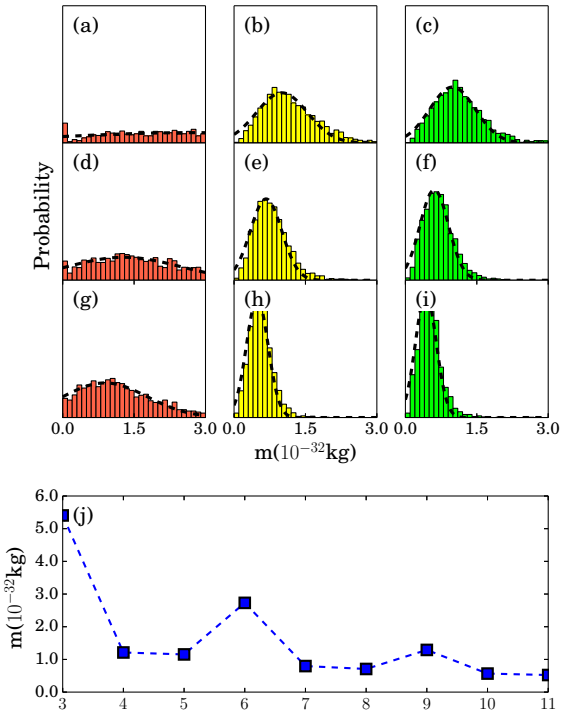

Fig. 7 (Color online)(a-i) Probability distributions of m of $N \times N$ cells (N=3,4,...,11). (j) The mean values of each ensemble.

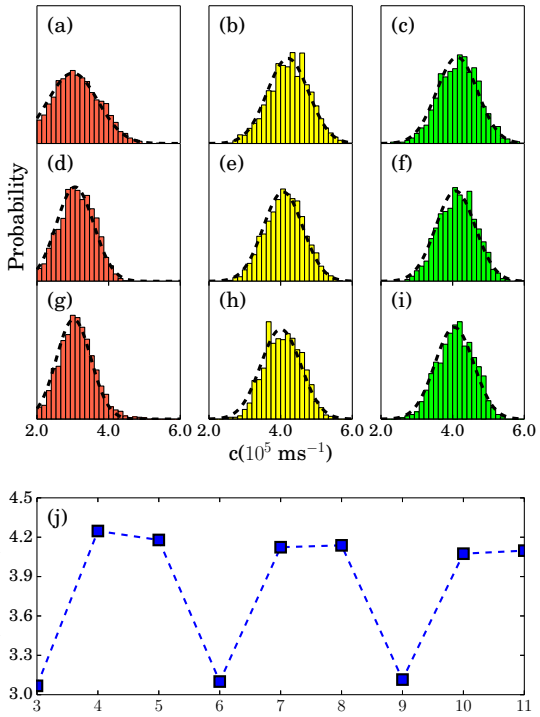

Fig. 8 (Color online) (a-i) Distribution of the effective speed of light of $N \times N$ cells. (j) The mean values of each ensemble.

The peak of the gap distribution shifts left and the distribution become narrower. However, in the $3p \times 3p$ supercell, there exists a much more significant intervalley scattering. Therefore, an abnormality occurs in the $3p \times 3p$ supercell. The gap of $3p \times 3p$ supercell is larger than that of $(3p-1) \times (3p-1)$ supercell with the same p. Nevertheless, the general trend that gap decrease with the increase of N is still clear among each group of $3p$(Fig.6(a)(d)(g)), $3p+1$(Fig.6(b)(e)(h)) and $3p+2$(Fig.6(c)(f)(i)) supercells.

The quantitative evaluation of the variation of band gaps can be done by the analysis of the average values. As shown in Fig.6 (j), the band gap variation have the periodicity of three. Each row (3p+1, 3p+2, 3p+3) in Fig.6(a-i) forms a group p(p=1,2,3.....). For each group p, the gaps of the three supercells have the relation $3p+2 < 3p+1 < 3p+3$. With the increase of p, the average gap of the group p decreases. It is predicted that the gap is extrapolated to zero at some N. This means that the randomly buckled silicene sheet with $N \to \infty$ become semimetal again, the same as the pristine silicene. The effect of buckling disorder on the silicene gap is smeared out.

Although the disorder generates a mass to the Dirac fermions, the mass is rather small. As shown in Fig.7, the m ranges from $7.6 \times 10^{-33} kg$ to $5.3 \times 10^{-32} kg$. It is only 1/100 of the mass of free electron, which makes the randomly buckled silicene much better than the traditional semiconductors to build high-speed electronic devices.

The masses of Dirac fermions m show the similar tendency of the variation of gaps as a function of N. It is worth noting that the abnormality of $3p \times 3p$ supercell is more obvious. For example, the mean value $\langle m \rangle$ of 6×6 silicene is about three times larger than that of 5×5 silicene. The difference between $N = 3p$ and $N \neq 3p$ decreases rapidly with p increases. The effect of buckling disorder on m is also smeared out as in the gap statistics when the size of silicene increases.

The similar analysis is carried on the statistics of effective speed of light, as shown in Fig.8. Similar to the band gaps, the $3p \times 3p$ supercell also shows speciality in Fermi velocity. The effective speed of light c of $3p \times 3p$ is abnormally low. This is also due to the existence of strong intervalley scattering.

The effective speed of light of the pristine silicene is from $5.27 \times 10^5 m/s$ to $6.75 \times 10^5 m/s$ with different types of exchange-correlation functional.[21] The mean value $\langle c \rangle$ in the randomly buckled $N \neq 3p$ silicene is only 14% lower than that of the pristine silicene.

From the results of the gap, mass and effective speed of light c, we demonstrate that the effects of buckling disorder become weaker as N increases. **In general, with N increases, the strength of the intervalley scattering decreases. Thus, $(N+1) \times (N+1)$ cell is more similar to the pristine silicene than $N \times N$ cell, which means that the $(N+1) \times (N+1)$ cell**

has smaller gap, lighter electron mass and higher effective speed of light than those of the $N \times N$ cell. However, in the $3p \times 3p$ supercell, because the Dirac point is folding to the Γ point, there exists a much more significant intervalley scattering.[62] The strong intervalley scattering causes larger gap, heavier electron mass and smaller effective speed of light. Therefore, an abnormality occurs in the $3p \times 3p$ supercell, which shows a periodicity of three in the distributions of energy gap, mass and effective speed of light.

The band structures near the Fermi level are protected by the AB sublattice symmetry. The symmetry breaking caused by the buckling disorder of one cell may be compensated by another cell. When N is small, the probability of the generation of the compensated structure is small. **With the $N \to \infty$, the probability become large and the average effect on the silicene will eventually vanish. This indicates that the infinite silicene sheet shares the similar properties with the pristine silicene. Thus, it is predicted that the buckling disorder may not change the properties obtained from pristine silicene, such as the semimetal band structure, the high mobility of the quasiparticles, the topological gap[18] and the band structures of hydrogenated and lithiated silicene[63–65].**

3.3 Energy gap with electric field

The essential condition to build FET devices using silicene is the generation of a gap. The application of electric field is a commonly used method. In the followings, we show the effect of the electric field on randomly buckled silicene. The tight-binding Hamiltonian with the electric field is also described by Eq. (1), where the $H_{i,i}$ become[20]

$$H_{i,i} = \begin{pmatrix} \varepsilon_s + eEz & 0 & 0 & 0 \\ 0 & \varepsilon_p + eEz & 0 & 0 \\ 0 & 0 & \varepsilon_p + eEz & 0 \\ 0 & 0 & 0 & \varepsilon_p + eEz \end{pmatrix} \tag{10}$$

instead of Eq. (2), where E is the electric field in Z direction, e is the charge of the electron and z is the hight in Z direction.

A large electric field is needed to generate a sufficient gap in pristine silicene at zero temperature.[20,21] To investigate systemically the thermal effect together with the electric field E on the silicene, we calculate the electronic properties of the 8×8 silicene with different E and different temperature T. An electric field varies from $0.01V/Å$ to $0.1V/Å$ is applied to the 8×8 supercells at 0K, 150K, 300K and 450K. $N = 2000$ structures are sampled using the Metropolis algorithm for each situation.

The gap statistics of the 8×8 silicene ensemble at 300K is shown in Fig. 9(a-i). As the electric field increases, the peak shifts right. The gaps change linearly with the electric field, as shown in Fig. 9(j). At 0K, the buckling heights in silicene

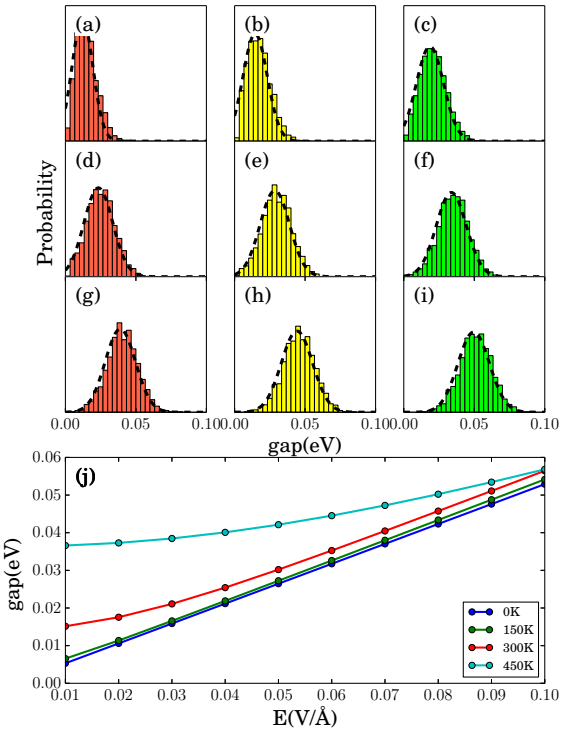

Fig. 9 (Color online) (a-i) Distributions of the gaps of 8×8 cell with $E = 0.01 - 0.09V/Å$ at 300K. (j) The mean value of each ensemble at 0K, 150K, 300K and 450K.

become ordered. The relation between gap Δ and electric field E at 0K is consistent with the former study.[20] The $\Delta(E)$ curve at 150K is almost the same to the 0K curve with only a small shift upward. At 300K and 450K, the shifts are more obvious. A higher temperature causes a larger gap for the same E. To generate a band $\Delta = 37meV$ at 0K, an electric field $E = 0.7V/\AA$ is needed while only $E = 0.1V/\AA$ is needed at 450K. It means that compared with the pristine silicene, the randomly buckled silicene need much smaller electric field to generate the same gap. The main reason is that the average buckling height becomes larger in the thermal field, which increases z in Eq. (9). Therefore, the symmetry between AB sublattices are easier to be broken in a small electric field.

4 Summary

In summary, we have investigated the effect of thermal field on the electronic properties of silicene. The vibration in buckling height is the main Goldstone mode while the in-plane movement is frozen at room temperature. The randomly buckled structure due to thermal fluctuation is used to simulate the silicene at nonzero temperature. The long time average of the electronic structure of silicene can be described by an ensemble which consist of numerous randomly buckled structures. Using the finite-size scaling approach, $N \times N(N = 1, 2.....)$ supercells are calculated and the property of the realistic silicene material is predicted by extrapolation to the limit $N \to \infty$. From the statistics of the gaps, the masses of Dirac fermions and the effective speed of light as a function of N, we conclude that the effect of buckling disorder is smeared out as $N \to \infty$. Thus, the randomly buckled silicene shares almost the same electronic properties as pristine silicene. Moreover, to generate a band gap, the randomly buckled silicene need much smaller electric field than the pristine silicene. The higher temperature corresponds to a larger gap under the same electric field. All these features of silicene have a great application potential for electronic devices at room temperature.

5 Acknowledgement

This research was supported by the National Science Foundation of China (Grant Nos. 11174171 and 11374175).

References

1 B. Lalmi, H. Oughaddou, H. Enriquez, A. Kara, S. Vizzini, B. Ealet and B. Aufray, *Appl. Phys. Lett.*, 2010, **97**, 223109–223109.
2 L. Chen, H. Li, B. Feng, Z. Ding, J. Qiu, P. Cheng, K. Wu and S. Meng, *Phys. Rev. Lett.*, 2013, **110**, 085504.
3 P. Vogt, P. De Padova, C. Quaresima, J. Avila, E. Frantzeskakis, M. C. Asensio, A. Resta, B. Ealet and G. Le Lay, *Phys. Rev. Lett.*, 2012, **108**, 155501.
4 B. Feng, Z. Ding, S. Meng, Y. Yao, X. He, P. Cheng, L. Chen and K. Wu, *Nano Lett.*, 2012, **12**, 3507–3511.
5 P. De Padova, O. Kubo, B. Olivieri, C. Quaresima, T. Nakayama, M. Aono and G. Le Lay, *Nano Lett.*, 2012, **12**, 5500–5503.
6 H. Enriquez, S. Vizzini, A. Kara, B. Lalmi and H. Oughaddou, *J. Phys.: Condens. Matter*, 2012, **24**, 314211.
7 H. Jamgotchian, Y. Colignon, N. Hamzaoui, B. Ealet, J. Y. Hoarau, B. Aufray and J. P. Bibian, *J. Phys. Condens. Matter*, 2012, **24**, 172001.
8 C.-L. Lin, R. Arafune, K. Kawahara, N. Tsukahara, E. Minamitani, Y. Kim, N. Takagi and M. Kawai, *Appl. Phys. Express*, 2012, **5**, 045802.
9 B. Feng, H. Li, C.-C. Liu, T.-N. Shao, P. Cheng, Y. Yao, S. Meng, L. Chen and K. Wu, *ACS nano*, 2013, **7**, 9049–9054.
10 L. Chen, B. Feng and K. Wu, *Appl. Phys. Lett.*, 2013, **102**, 081602.
11 A. Resta, T. Leoni, C. Barth, A. Ranguis, C. Becker, T. Bruhn, P. Vogt and G. Le Lay, *Sci. Rep.*, 2013, **3**, year.
12 Z. Majzik, M. R. Tchalala, M. Švec, P. Hapala, H. Enriquez, A. Kara, A. J. Mayne, G. Dujardin, P. Jelínek and H. Oughaddou, *J. Phys.: Condens. Matter*, 2013, **25**, 225301.
13 N. W. Johnson, P. Vogt, A. Resta, P. De Padova, I. Perez, D. Muir, E. Z. Kurmaev, G. Le Lay and A. Moewes, *Adv. Funct. Mater.*, 2014, **24**, 5253–5259.
14 Y. Du, J. Zhuang, H. Liu, X. Xu, S. Eilers, K. Wu, P. Cheng, J. Zhao, X. Pi, K. W. See *et al.*, *ACS nano*, 2014.
15 Z.-L. Liu, M.-X. Wang, J.-P. Xu, J.-F. Ge, G. Le Lay, P. Vogt, D. Qian, C.-L. Gao, C. Liu and J.-F. Jia, *New. J. Phys*, 2014, **16**, 075006.
16 M. R. Tchalala, H. Enriquez, H. Yildirim, A. Kara, A. J. Mayne, G. Dujardin, M. A. Ali and H. Oughaddou, *Appl. Surf. Sci.*, 2014, **303**, 61–66.
17 R. Friedlein, A. Fleurence, K. Aoyagi, M. de Jong, H. Van Bui, F. Wiggers, S. Yoshimoto, T. Koitaya, S. Shimizu, H. Noritake *et al.*, *J. Chem. Phys.*, 2014, **140**, 184704.
18 C. Liu, W. Feng and Y. Yao, *Phys. Rev. Lett.*, 2011, **107**, 076802.
19 A. Kara, H. Enriquez, A. Seitsonen, L. Lew Yan Voon, S. Vizzini, B. Aufray and H. Oughaddou, *Surf. Sci. Rep.*, 2012, **67**, 1 – 18.
20 Z. Ni, Q. Liu, K. Tang, J. Zheng, J. Zhou, R. Qin, Z. Gao, D. Yu and J. Lu, *Nano Lett.*, 2012, **12**, 113–118.
21 N. D. Drummond, V. Zólyomi and V. I. Fal'ko, *Phys. Rev. B*, 2012, **85**, 075423.
22 J. Gao, J. Zhang, H. Liu, Q. Zhang and J. Zhao, *Nanoscale*, 2013, **5**, 9785–9792.
23 Y.-P. Wang and H.-P. Cheng, *Phys. Rev. B*, 2013, **87**, 245430.
24 K. Zberecki, R. Swirkowicz, M. Wierzbicki and J. Barnaś, *Phys. Chem. Chem. Phys.*, 2014, **16**, 12900–12908.
25 Y.-C. Zhao and J. Ni, *Phys. Chem. Chem. Phys.*, 2014, **16**, 15477–15482.
26 N. Gao, J. C. Li and Q. Jiang, *Phys. Chem. Chem. Phys.*, 2014, **16**, 11673–11678.
27 H. Liu, J. Gao and J. Zhao, *J. Phys. Chem. C*, 2013, **117**, 10353–10359.
28 R.-W. Zhang, C.-W. Zhang, W. Ji, S.-j. Hu, S. Yan, S. Li, P. Li, P. Wang and Y.-S. Liu, *J. Phys. Chem. C*, 2014.
29 C.-C. Lee, A. Fleurence, R. Friedlein, Y. Yamada-Takamura and T. Ozaki, *Phys. Rev. B*, 2013, **88**, 165404.
30 L. Li and M. Zhao, *J. Phys. Chem. C*, 2014, **118**, 19129–19138.
31 H. Shu, D. Cao, P. Liang, X. Wang, X. Chen and W. Lu, *Phys. Chem. Chem. Phys.*, 2014, **16**, 304–310.
32 C. Lian and J. Ni, *AIP Adv.*, 2013, **3**, 052102.
33 H. Liu, N. Han and J. Zhao, *J. Phys.: Condens. Matter*, 2014, **26**, 475303.
34 H. Fu, J. Zhang, Z. Ding, H. Li and S. Meng, *Appl. Phys. Lett.*, 2014, **104**, 131904.
35 J. Liu and W. Zhang, *RSC Adv.*, 2013, **3**, 21943–21948.
36 E. H. Song, S. H. Yoo, J. J. Kim, S. W. Lai, Q. Jiang and S. O. Cho, *Phys. Chem. Chem. Phys.*, 2014, **16**, 23985–23992.
37 B. Huang, H.-X. Deng, H. Lee, M. Yoon, B. G. Sumpter, F. Liu, S. C. Smith and S.-H. Wei, *Phys. Rev. X*, 2014, **4**, 021029.

38 L. Tao, E. Cinquanta, D. Chiappe, C. Grazianetti, M. Fanciulli, M. Dubey, A. Molle and D. Akinwande, *Nature nanotechnology*, 2015.

39 A. Fasolino, J. Los and M. I. Katsnelson, *Nat. Mater.*, 2007, **6**, 858–861.

40 Z.-X. Guo and A. Oshiyama, *Phys. Rev. B*, 2014, **89**, 155418.

41 M. P. Lima, A. Fazzio and A. J. R. da Silva, *Phys. Rev. B*, 2013, **88**, 235413.

42 C.-L. Lin, R. Arafune, K. Kawahara, M. Kanno, N. Tsukahara, E. Minamitani, Y. Kim, M. Kawai and N. Takagi, *Phys. Rev. Lett.*, 2013, **110**, 076801.

43 G. Kresse and J. Hafner, *Phys. Rev. B*, 1993, **47**, 558–561.

44 G. Kresse and J. Hafner, *Phys. Rev. B*, 1994, **49**, 14251–14269.

45 G. Kresse and J. Furthmüller, *Phys. Rev. B*, 1996, **54**, 11169–11186.

46 P. E. Blöchl, *Phys. Rev. B*, 1994, **50**, 17953–17979.

47 J. P. Perdew, K. Burke and M. Ernzerhof, *Phys. Rev. Lett.*, 1996, **77**, 3865–3868.

48 H. Monkhorst and J. Pack, *Phys. Rev. B*, 1976, **13**, 5188–5192.

49 J. Slater and G. Koster, *Phys. Rev.*, 1954, **94**, 1498.

50 H. Ochoa, A. C. Neto, V. Fal'ko and F. Guinea, *Phys. Rev. B*, 2012, **86**, 245411.

51 C.-C. Liu, H. Jiang and Y. Yao, *Phys. Rev. B*, 2011, **84**, 195430.

52 C.-C. Liu, S. Guan, Z. Song, S. A. Yang, J. Yang and Y. Yao, *arXiv preprint arXiv:1402.5817*, 2014.

53 M. Zhou, W. Ming, Z. Liu, Z. Wang, Y. Yao and F. Liu, *arXiv preprint arXiv:1401.3392*, 2014.

54 H. Min, J. Hill, N. A. Sinitsyn, B. Sahu, L. Kleinman and A. H. MacDonald, *Phys. Rev. B*, 2006, **74**, 165310.

55 J. Mintmire and C. White, *Phys. Rev. Lett.*, 1998, **81**, 2506.

56 V. Pereira, A. Neto and N. Peres, *Phys. Rev. B.*, 2009, **80**, 045401.

57 L. Goodwin, A. Skinner and D. Pettifor, *Europhys. Lett.*, 1989, **9**, 701.

58 W. H. Press, S. A. Teukolsky, W. T. Vetterling and B. P. Flannery, *Numerical Recipes in C++*, Cambridge university press, 2002.

59 D. P. Landau and K. Binder, *A guide to Monte Carlo simulations in statistical physics*, Cambridge university press, 2009.

60 A. Geim and K. Novoselov, *Nat. Mater.*, 2007, **6**, 183–191.

61 M. Hasan and C. Kane, *Rev. Mod. Phys.*, 2010, **82**, 3045–3067.

62 H. Jiang, Z. Qiao, H. Liu, J. Shi and Q. Niu, *Phys. Rev. Lett.*, 2012, **109**, 116803.

63 L. C. Lew Yan Voon, E. Sandberg, R. S. Aga and A. A. Farajian, *Applied Physics Letters*, 2010, **97**, –.

64 T. H. Osborn, A. A. Farajian, O. V. Pupysheva, R. S. Aga and L. L. Y. Voon, *Chemical Physics Letters*, 2011, **511**, 101 – 105.

65 T. H. Osborn and A. A. Farajian, *The Journal of Physical Chemistry C*, 2012, **116**, 22916–22920.